Bifurcation study of regular pulse packages in laser diodes subject to optical feedback

Andrzej Tabaka,[1,*] Krassimir Panajotov,[1,†] Irina Veretennicoff,[1] and Marc Sciamanna[2]
[1]*Department of Applied Physics and Photonics (TW-TONA), Vrije Universiteit Brussel (VUB), B-1050 Brussels, Belgium*
[2]*Supélec - Ecole Supérieure d'Electricité, 2 Rue Edouard Belin, F-57070 Metz, France*
(Received 10 February 2004; published 27 September 2004)

We study the influence of delayed optical feedback from a short external cavity on the emission dynamics of semiconductor lasers using the Lang and Kobayashi rate equation model. A combination of numerical integration and continuation techniques allows us to bring new light into the bifurcation scenario leading to the regular pulse packages (RPP) regime. We give examples of bistability between RPP and time-periodic or steady state solutions. Our bifurcation study of RPP regime is complemented by an analysis of the dependency of the RPP period on the laser and feedback parameters. We qualitatively study this new dynamical regime by plotting a two-dimensional map in the feedback parameters space. The occurrence of RPP is furthermore associated with a topological change in the bifurcation diagram and accompanied by the creation of a new type of bifurcation bridge between a mode and an antimode.

DOI: 10.1103/PhysRevE.70.036211 PACS number(s): 05.45.−a, 42.65.Sf

I. INTRODUCTION

When inserted in any optical system, semiconductor lasers (SLs) are inevitably subject to optical feedback (OF), i.e., external reflection of the light which re-enters the laser cavity after a certain delay time. Such time-delayed OF might significantly affect the stable laser operation and induce complex dynamics, such as self-pulsations [1], multistability [2] and chaos [3,4]. For most applications in which a stable laser operation is indispensable, i.e., in data transmission, the instabilities induced by OF must be avoided by means of expensive optical isolators. Alternatively, high sensitivity of SLs to OF can also be used in a constructive way: optical feedback can narrow the linewidth of the emitted light [5,6] and may also be used for chaotic encryption [7], optical data readout and frequency tuning [8,9].

Most of the theoretical analysis of the influence of delayed OF from an external cavity (EC) on the emission dynamics of SL is based on the Lang-Kobayashi (LK) approach [10]. It accounts for one longitudinal laser mode and one roundtrip in the EC. In dimensionless form the LK equations read [11]

$$\dot{E}(s) = (1 + i\alpha)NE(s) + \eta e^{-i\omega\theta}E(s - \theta), \tag{1}$$

$$T\dot{N} = J - N - (1 + 2N)|E(s)|^2, \tag{2}$$

where $E(s) = \sqrt{P(s)}e^{i\phi(s)}$, stands for the electric field, P and ϕ being the power and the phase of the light wave, and N is the excess carrier number. In these equations, the dimensionless time s is in units of photon lifetime $\tau_p (s \equiv t/\tau_p)$. The parameters T and θ are defined as $T \equiv \tau_n/\tau_p$ and $\theta \equiv \tau/\tau_p$ where τ_n and τ are the carrier lifetime and the external round-trip time, respectively. $\omega \equiv \omega_0\tau_p$ and $\eta \equiv \gamma\tau_p$ are the dimensionless angular frequency of the solitary laser and the feedback rate, respectively. J is the excess pump current proportional to $(J_0/J_{\text{th,sol}} - 1)$ and α is the linewidth enhancement factor. The steady-state solutions of these equations are the so-called external cavity modes (ECMs). In the $[\phi(s) - \phi(s-\theta), N]$ plane, ECMs lie on an ellipse given by the equation [12]

$$(\phi(s) - \phi(s - \theta) - \alpha\theta N)^2 + (\theta N)^2 = (\eta\theta)^2. \tag{3}$$

The right-hand side of Eq. (3), i.e., the product of the feedback strength η and the delay θ, determines the characteristics of this ellipse and the number of existing ECMs. It is well known that as we increase this product, ECMs appear in pairs through saddle-node bifurcation and one of the newly created ECMs is potentially stable (and therefore called *mode*) and the other one is always unstable (called *antimode*). The stable modes are located in the lower branch of the ellipse, whereas antimodes are situated in the upper one.

Extensive experimental and theoretical investigations over the last three decades show that qualitatively different dynamical regimes are observed depending on the feedback strength η [13] and/or the length of the EC [14]. Usually, we say that the length of the EC is long (short) if the corresponding EC round trip time θ is larger (smaller) than the relaxation oscillation period $T_{\text{RO}} \equiv \pi\sqrt{2T/J}$ [14,15]. In the case of long EC and moderate feedback rates, the stable emission of the SL is easily destabilized and chaotic regimes arise. Typically observed chaotic dynamics in the long cavity regime are the so-called low-frequency fluctuations (LFF) [16,17], which manifest as sporadic and sudden dropouts of the light intensity followed by successive, much slower stepwise return to maximal power. The regime of LFF anticipates another intriguing regime that is the coherence collapse (CC) regime [18]. It is usually found by either increasing the pump current or increasing the EC delay time once the LFF regime was found. CC can be recognized by a significant broadening of the optical linewidth up to a few tens of GHz.

In contrast to these long EC feedback instabilities, short EC dynamics is expected to be less complicated because of

*Electronic address: atabaka@tona.vub.ac.be
†Also at Institute of Solid State Physics, 72 Tzarigradsko Chaussee Blvd., 1784 Sofia, Bulgaria.

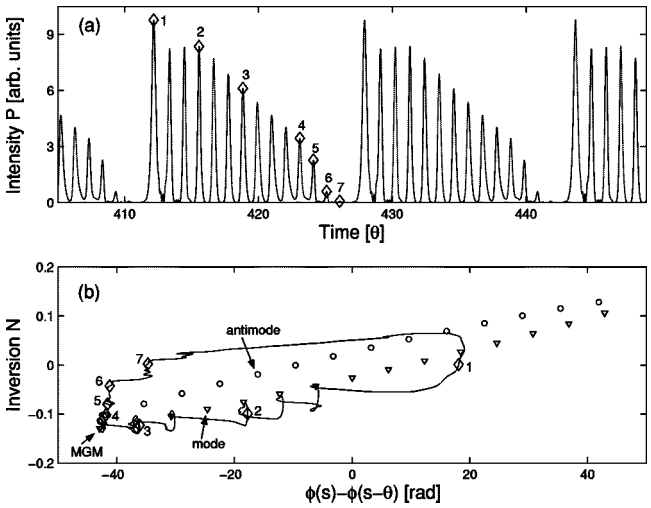

FIG. 1. Numerically computed trajectory in the RPP dynamics using the LK model. We have plotted in (a) the time trace of intensity P variations in time measured in units of the delay θ and in (b) phase portrait in the $[\phi(s)-\phi(s-\theta),N]$ space. Modes are represented by triangles and antimodes by circles. Numbers indicate distinct moment in time during RPP. The parameters are $J=1.155$, $\eta=0.135$, $\theta=70$, $\alpha=5$, and $\omega\theta=-\arctan\alpha$.

the reduced number of ECMs. However, lasers with short external cavity have recently been found to exhibit interesting dynamics. For example, it has been shown theoretically in Refs. [14,19] that laser diodes with short EC can generate microwave oscillations of the emitted power due to a beating between a stable ECM and an antimode. Also stable oscillations corresponding to a beating between two stable ECMs [20–22], high frequency pulsating solutions emerging from a subcritical Hopf bifurcation [23,24] and chaotic dynamics [25] have been reported in SL with short EC feedback.

In this paper we analyze another dynamical behavior of laser diodes subject to short EC optical feedback, which is called regular pulse packages or RPP. We build upon unprecedented insight into the dynamics in short EC that was presented in Refs. [15,26]. We remind the reader of the RPP dynamics in Fig. 1. It corresponds to the emission of high intensity pulses separated by the delay time θ and that are modulated by a slower, time-periodic envelope; see Fig. 1(a). During one RPP cycle the system follows the same path visiting different ECMs in the direction to the maximum gain ECM (MGM); see Fig. 1(b). Then the laser system is repelled across the unstable branch of the ECM ellipse inducing the phase shift to the direction of ECM with larger N. Heil *et al.* in Ref. [15] briefly compared the RPP dynamics with the dynamics observed in the LFF regime. In both cases, low frequency phenomena are present connected with a global trajectory along several attractor ruins and producing pulses when visiting each of them. What makes RPP distinct from LFF is the sensitivity to phase of the back-reflected light [26]. The transition from RPP to LFF occurs when the delay becomes larger than the RO period.

In this paper we throw more light into the bifurcation origin and the main dynamical properties of the RPP regime. In Sec. II we numerically investigate the bifurcation transition to RPP dynamics, i.e., the qualitatively different dynamics that are involved. Our analysis allows us to unveil different cases of bistability between RPP and steady-state or time-periodic dynamics and also shows that the slow envelope of RPP may experience several period-doubling bifurcations. As we increase the feedback rate, the windows of RPP progressively merge to a continuous region of RPP, which we analyze in more details through a two-dimensional map in the plane of the feedback parameters in Sec. III. We reveal that the largest region of RPP occurs "in the middle of the short EC regime," i.e., for values of the EC delay time close to half of the RO period. Hereafter, we also analyze how the interplay between the system trajectory in the phase space and the creation of new ECMs governs the dependency of the period of the pulse package envelope on the laser and feedback parameters. Finally, a computation of the unstable branches of steady-state and time-periodic solutions in Sec. IV allows us to relate the occurrence of RPP dynamics with the destruction of a Hopf bifurcation bridge between a mode and an antimode and the creation of a new mode-antimode bridge with a different topology. Our results are summarized in Sec. V.

II. BIFURCATION TRANSITION TO RPP

The bifurcation transition leading to RPP dynamics is analyzed in Figs. 2 and 3. We take the feedback rate η as a bifurcation parameter while the other parameters remain fixed. Figure 2 shows time traces of the intensity P [panels (1)] and the corresponding phase portraits of the excess carrier number N as a function of phase difference $\phi(s)-\phi(s-\theta)$ [panels (2)]. As we already mentioned in Sec. I, ECMs appear in pairs of modes and antimodes as we increase η and they lie on an ellipse in the phase space. The modes are represented by triangles and the antimodes by circles. In Fig. 3 we plot the bifurcation diagrams of the laser intensity, i.e., the successive extrema of the laser intensity as we vary the feedback rate η upwards [Fig. 3(a)] and downwards [Fig. 3(b)], respectively. The labels in Fig. 3 refer to the dynamics analyzed in Fig. 2.

We start our bifurcation analysis from the time periodic solution shown in Fig. 2(a) and which has emerged from the destabilization of the MGM through a Hopf bifurcation; see also Fig. 3. When increasing the feedback rate η the time-periodic solution destabilizes to quasiperiodic dynamics [Fig. 2(b)], i.e., the system trajectory lies on a torus which is restricted to the nearest area around the destabilized MGM. In Fig. 3 this quasiperiodic attractor (label b) is hidden by the irregular pulse package dynamics (label c).

We find that for the same η the quasiperiodic solution [Fig. 2(b)] may coexist with a qualitatively different dynamics in which the laser emits packages of pulses [Fig. 2(c)]. The laser intensity exhibits pulsations at the EC frequency, which are modulated by a slower envelope. In the time of the pulse package, ECMs are visited in direction to the MGM. In the vicinity of the MGM, the phase trajectory spirals many times around the compound cavity modes while being shifted towards antimodes after each spiralling motion. The system trajectory then collides with an antimode and is suddenly repelled towards the center of the ellipse [Fig. 2(c2)].

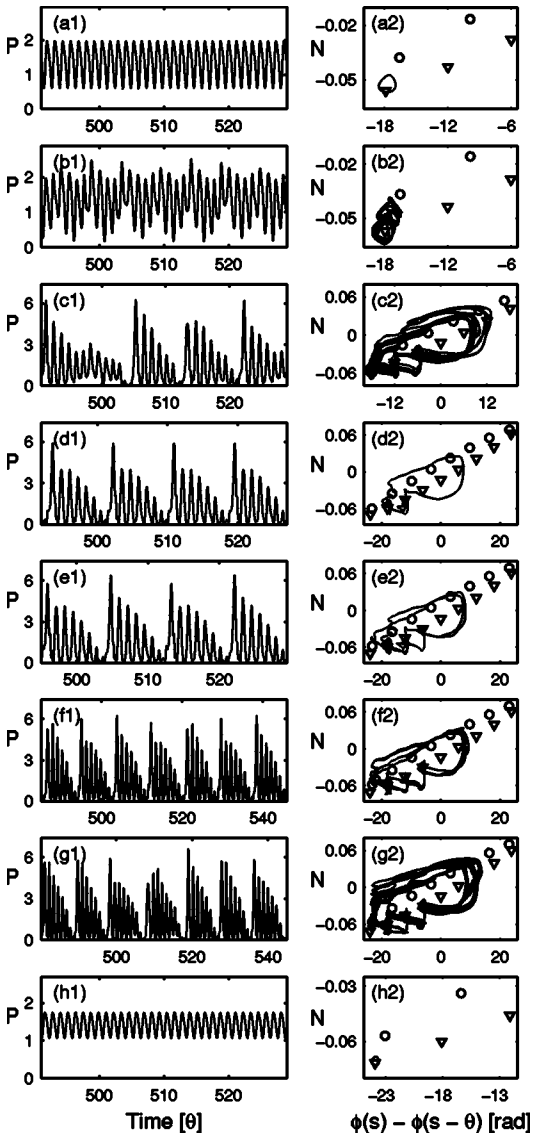

FIG. 2. Time traces of intensity P variations in time [panels (1)] measured in units of the delay θ and phase portraits [panels (2)] in the $[\phi(s)-\phi(s-\theta),N]$ space showing the development and disappearing of RPP. Modes are represented by triangles and antimodes by circles. In (a) $\eta=0.061$, (b) and (c) 0.064, (d) 0.0688, (e) 0.0707, (f) 0.0715, (g) and (h) 0.073, respectively. The parameters are $J=1.15$, $\theta=70$, $\alpha=5$, and $\omega\theta=-\arctan\alpha$.

Quite similar type of dynamics has also been observed for the case of the long external cavity chaotic LFF regime [27]. This dynamics appears all of a sudden and has been associated with an interior crisis [28] of the laser system in which a sudden increase of the size of a chaotic attractor takes place; see (b) and (c) in Figs. 2 and 3. What makes RPP unique is that in RPP the collision always takes place in the vicinity of the same compound cavity mode whereas in the LFF case the antimode which initiates the collision changes from one LFF cycle to another one. The bifurcation diagram in Fig. 3(a) suggests also a presence of a boundary crisis in the system [28] which causes a sudden disappearance of RPP dynamics as η is increased; see (g) and (h) in Figs. 2 and 3.

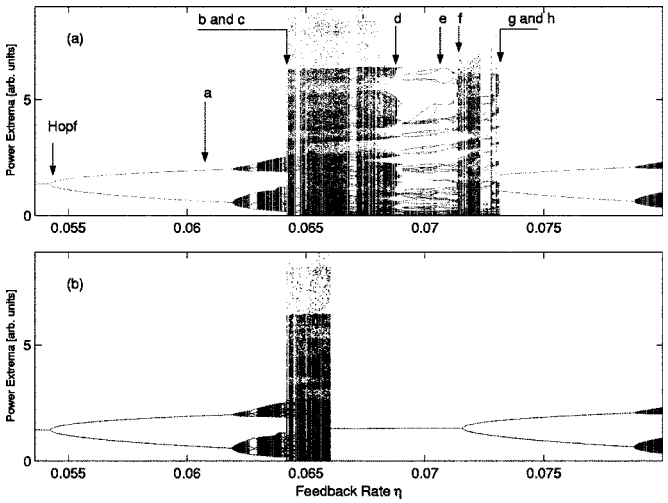

FIG. 3. Extrema of the laser intensity as a function of the feedback rate η. The figure shows a representation of different dynamical regimes in the form of the bifurcation diagram. The feedback rate was first (a) increased and then (b) decreased. Arrows indicate the dynamical situations from Fig. 2. In (a) $\eta=0.061$, (b) and (c) 0.064, (d) 0.0688, (e) 0.0707, (f) 0.0715, (g) and (h) 0.073, respectively. The parameters are $J=1.15$, $\theta=70$, $\alpha=5$, and $\omega\theta=-\arctan\alpha$.

Since there is not a clear borderline between those two short and long dynamical regimes there must be a continuous transition from short to long external cavity regime. This transition is accompanied with progressive change of the shape of the pulse packages envelope followed by progressive lack of periodicity [24,29]. This transition roughly occurs when θ is close to the RO period [15], which for our parameters is close to 170. In Fig. 2(c) the pulse packages are not yet regular. With further increase of η the quasiperiodic attractor disappears and RPP is observed; see Fig. 2(d). In the RPP regime the laser system always follows the same trajectory in the phase space visiting only some ECMs. This RPP regime corresponds to the label (d) in Fig. 3. Since the maxima of the pulses are always at the same intensity level from pulse package to pulse package, the occurrence of continuous regions of RPP yields a set of parallel lines in the bifurcation diagram.

With increasing the feedback strength RPP may undergo a period doubling bifurcation cascade. Period-two RPP, i.e., first RPP repeats every two cycles, is shown in Fig. 2(e) and period-four RPP is shown in Fig. 2(f). These domains of period doubling are indicated, respectively, by (e) and (f) in Fig. 3. As we further increase η, the regularity of the pulse packages is destroyed as depicted in Fig. 2(g) and indicated by label (g) in Fig. 3. These irregular pulse packages coexist with a time-periodic solution that originates from a newly born ECM [Fig. 2(h) and label (h) in Fig. 3]. The region of bistability is better observed when comparing the bifurcation diagrams in Fig. 3(a) and 3(b). As can be seen from Fig. 3(b) decreasing the feedback rate η from periodic solution (h) brings the system to this newly born ECM steady state through the Hopf bifurcation and the system stays in the MGM until the mode disappears and the system enters the chaotic regime.

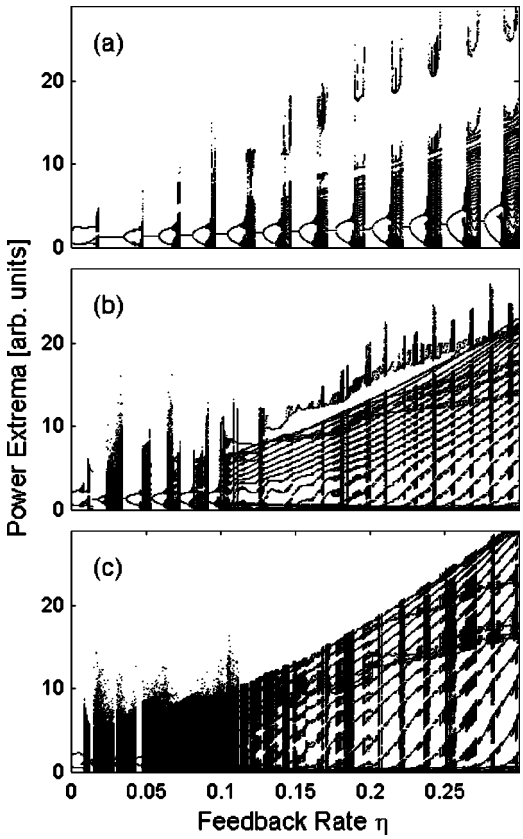

FIG. 4. Bifurcation diagrams of the laser intensity P as a function of the feedback rate η for different delay θ. In (a) $\theta=50$, (b) 70, and (c) 90. The parameters are $J=1.155$, $\theta=70$, $\alpha=5$, and $\omega\theta=-\arctan\alpha$.

III. MAPPING OF THE RPP DYNAMICS

Figure 4 shows bifurcation diagrams of the laser intensity P as a function of η and for three different values of θ namely $\theta=50$, 70, and 90. In each case η was ramped from 0 to 0.3 in very fine increments. At each step the extrema of the output power were recorded after waiting for the transient to die out (about few tens of RPP cycles). If we compare the bifurcation diagrams for different values of θ we see that for small delays ($\theta=50$) the laser system undergoes the same cascade of bifurcations as presented in Figs. 2 and 3. When increasing the feedback rate η the laser system bifurcates from a steady state solution to a periodic state, then becomes quasiperiodic and possibly chaotic. The chaotic dynamics corresponds to irregular sequences of pulses which may become regular (RPP) for some values of η. As we increase η further, the system settles to a newly born ECM steady state and a cascade of bifurcations similar to the one presented in the preceeding section occurs. Here, the windows of RPP are initially narrow and broaden with increasing the feedback strength η [Fig. 4(a)]. For intermediate level of the delay $\theta=70$ [Fig. 4(b)] the windows of RPP expand and eventually merge as η increases giving a broad, continuous window of RPP. For larger delays ($\theta=90$) [Fig. 4(c)] we observe that RPP is destabilized at small feedback rates η giving rise to chaotic states and, moreover, the broad

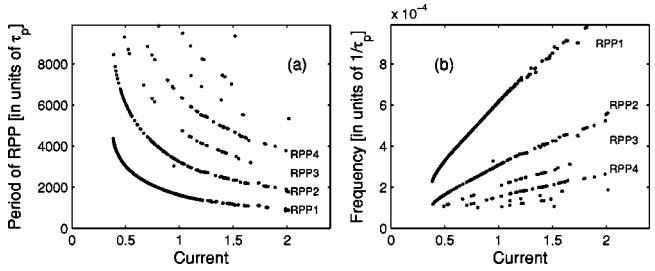

FIG. 5. Period (a) and frequency (b) of envelope of RPP as a function of injection current. Indices (RPP1), (RPP2), (RPP3) and (RPP4) indicate the order of the period of RPP. The parameters are $\eta=0.2$, $\theta=85$, $\alpha=5$, and $\omega\theta=-\arctan\alpha$.

window of RPP shrinks. The chaotic dynamics resembles very much the one of LFF when plotted in the phase space $[\phi(s)-\phi(s-\theta),N]$. This LFF type of dynamics starts to dominate and eventually for even larger delays it overtakes RPP.

We complement our observations by plotting a detailed map of RPP dynamics in the plane (θ,η). In order to plot this map we follow a similar procedure to the one used to plot bifurcation diagrams but this time we sweep the two bifurcation parameters, namely the feedback rate η and the delay time θ.

We develop an automatic way to detect the presence of regular pulse packages. For each pair of η, θ, we integrate the LK equations and analyze the time trace of laser intensity. As time goes on, we record the successive extrema and also keep in memory the largest maximum in the intensity time trace. We check if this maximum repeats at regularly spaced time intervals. In this case the dynamics is time periodic and a clock is activated to measure the period. Next, we check if the time-periodic dynamics corresponds to the RPP regime. To this end, we compute the number of intensity oscillations in the duration of one period, i.e., the number of successively different intensity maxima within one period. We know that if the dynamics corresponds to RPP then the laser emits pulses at each external-cavity round-trip time, such that the maximum number of pulses corresponds to the period of the pulse package divided by the delay time. We compare this approximate number of pulses with the one detected from the analysis of the simulated time trace and then with some tolerance we conclude whether the dynamics is RPP or just another type of time-periodic behavior. We also have access to the value of the RPP period (T_{RPP}).

As an example we plot the period (T_{RPP}) and the frequency ($\nu_{\mathrm{RPP}}=1/T_{\mathrm{RPP}}$) of RPP as a function of the injection current J in Fig. 5. We observe that with increasing the current the frequency (period) of RPP continuously increases (decreases). Interestingly, the dependency of the frequency is linear for large levels of injection currents as in Ref. [26] but for low levels of current the curve is significantly bent. We remind the reader that changing the current modifies the ratio of the two characteristic time scales in the system; i.e., the delay θ and the relaxation oscillation period T_{RO}. In other words, increasing the injection current can bring the system from short to long external cavity regime. Therefore, the linear scaling of $\nu_{\mathrm{RPP}}(J)$ for large pump current values seems to

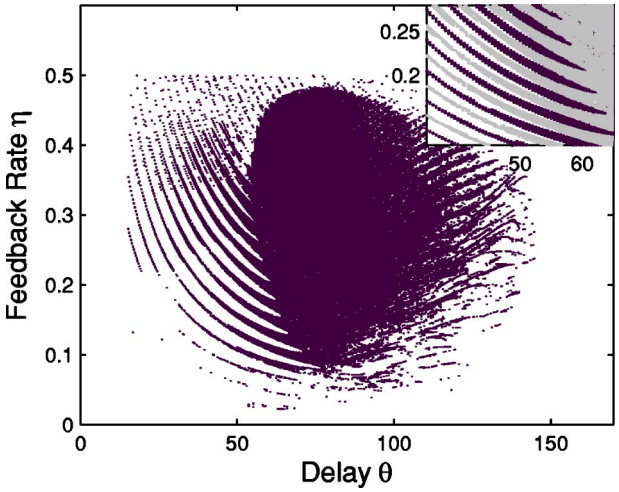

FIG. 6. Map of the RPP dynamics in the (θ, η) space. The parameters are $J=1.155$, $\alpha=5$, and $\omega\theta=-\arctan\ \alpha+\pi$. The inset illustrates the phase dependency of RPP: in black the map is plotted for $\omega\theta=-\arctan\ \alpha$ and in gray $\omega\theta=-\arctan\ \alpha+\pi$.

be connected to the fact that we approach the long external cavity regime. To support this statement, it is worth mentioning that, interestingly, the scaling of the inverse mean time between power dropouts in the chaotic long EC LFF regime was also shown to be linear [30].

Our procedure also allows us to distinguish between higher order periods, i.e., when the pulse envelope repeats with a period larger than the duration of a single pulse package. These higher-order RPP regimes are identified in Fig. 5 by the labels RPP1 for the period-one RPP, RPP2 for the period-two RPP, RPP3 for the period-three RPP and finally RPP4 for the period-four RPP. It should be pointed out that the period of RPP2 is not exactly twice the period of RPP1 since the pulse package envelope and hence the trajectory in the phase plane differs slightly from pulse package to pulse package.

In the two-dimensional map of Fig. 6 we only plot the point representing the detected RPP dynamics, including RPP of higher order periods (up to period of 10). In this way we obtain quite representative picture of the regions of the RPP dynamics. From Fig. 6 we see that the regions of RPP are very well defined in the (η, θ) space. Our map reveals that RPP dynamics appears for intermediate levels of feedback strength η and at delays θ smaller than the RO period T_{RO} (for our parameters $T_{\mathrm{RO}} \simeq 170$). This is in agreement with previous observations by Heil *et al.* [15,26] where they suggest that RPP disappears when the delay approaches the RO period and then the transition to LFF takes place. Moreover, in Fig. 6 we find that the largest region of RPP is for delays around half of the RO period.

For smaller delays small windows of RPP are very well identified in Fig. 6 [as also depicted in Fig. 4(a)]. Similar restricted regions in the (η, θ) plane in short external cavities were found in Ref. [31] for the case of chaotic behavior. We mention that when changing the phase of the back reflected light the structure of this part of the map may be significantly altered. When the phase changes by $\pm\pi$ the windows of RPP shift in such a way that they fit the space in the map where

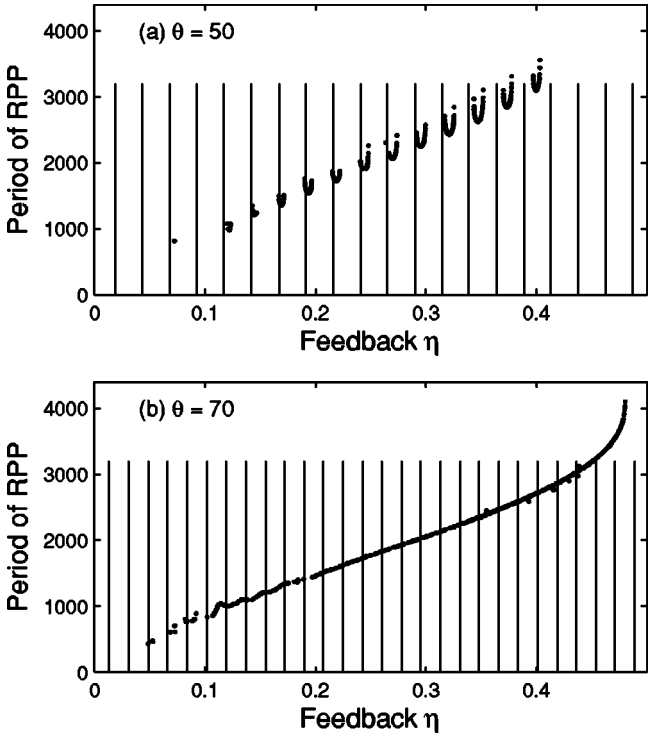

FIG. 7. Period of RPP in units of τ_p versus feedback strength η. In (a) $\theta=50$ and in (b) $\theta=70$. Vertical lines represent the value of η for which creation on new pair of ECMs takes place. The parameters are $J=1.155$, $\alpha=5$ and $\omega\theta=-\arctan\ \alpha$.

RPP was not previously present. We illustrate this phase sensitivity in the inset of Fig. 6 where we plot the regions of RPP for two different phase conditions that differ by π. We observe that changing the phase shifts the regions of RPP up and down such that RPP may be found in that interval of the (θ, η) space only if the proper phase condition is chosen. This agrees with the previous observations by Heil in Ref. [26] where they show that RPP is sensitive to optical phase. However, from the map we see that it is only true for small delays. For delay times larger than half the RO period the occurrence of RPP dynamics becomes phase insensitive. It is worth mentioning that the phase sensitivity in short EC optical feedback regime has been also observed both theoretically and experimentally in Ref. [25].

When the delay θ approaches half of the RO period, the windows of RPP broaden and merge as shown in Fig. 4(b). In such a way, the largest region of RPP occurs for delays around half of the RO period. When the delay θ approaches the RO period as shown in Fig. 4(c) the RPP loses synchronization and the dynamics becomes chaotic, similar to the one observed in the LFF regime; i.e., when averaged on a longer time scale, the laser intensity sporadically decreases and gradually returns to the original level. For larger delays the chaotic regime starts to dominate and therefore the windows of RPP shrink and finally disappear.

It is worth mentioning that the period of RPP depends not only on the injection current but also on the feedback parameters η and θ. For clarity reasons we will only focus on the lowest order RPP period (T_{RPP1}) in the following. In Fig. 7 we show the dependence of T_{RPP1} on the feedback strength η

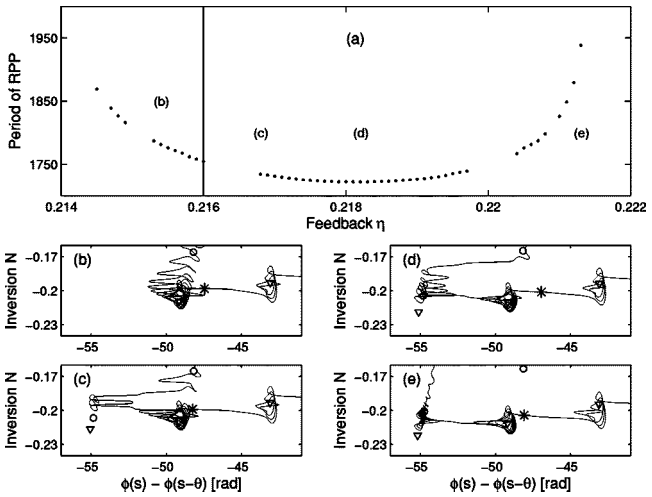

FIG. 8. An enlargement of Fig. 7(a) in the vicinity of the creation of ECMs together with a phase trajectory in the $[\phi(s)-\phi(s-\theta),N]$ space for different values of the feedback strength η. In (b) $\eta=0.2154$, (c) 0.2168 (d) 0.2182, and (e) 0.2213. The parameters are $J=1.155$, $\theta=50$, $\alpha=5$, and $\omega\theta=-\arctan\alpha$.

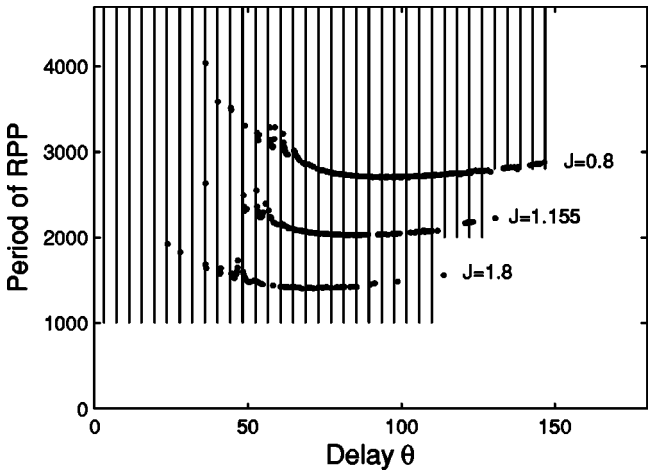

FIG. 9. Period of RPP in units of τ_p versus delay θ in units of τ_p for different values of the injection current. Vertical lines represent the value of θ for which creation on new pair of ECMs takes place. The parameters are $\eta=0.3$, $\alpha=5$, and $\omega\theta=-\arctan\alpha$.

for two values of the delay θ namely $\theta=50$ and $\theta=70$. In both cases we observe an increase of the period of T_{RPP1} with η which is associated with an increase of the number of ECMs and expansion of the ellipse. When increasing the feedback strength η the system visits more ECMs during one RPP cycle increasing the period. As already shown in Fig. 6, the regions of RPP are not continuous for small delays. At the moment RPP appears its period is very large, then it decreases and before the destabilization of RPP it increases again (forming a parabolalike curve). The straight vertical lines in Fig. 7 correspond to the exact values of the feedback η for which a creation of a new pair of ECMs takes place. We see that for the small feedback rate [Fig. 7(a)] the region of RPP starts before new ECMs are born and it proceeds even further away from that point. This indicates that RPP occurs due to destabilization of a previous MGM. Therefore, there is a region of bistability between RPP and the stable state. However, for large η the windows of RPP lie between two saddle-node bifurcations creating new ECMs.

It is interesting to investigate the mechanism that leads to this parabolic shape of T_{RPP1} in the vicinity of the creation of one new pair of ECMs; see Fig. 7(a). Here a creation of ECMs takes place around $\theta^*=0.216$. In Fig. 8(a) we plot the zoom of Fig. 7(a) in the vicinity of θ^* together with the phase trajectory in the $[\phi(s)-\phi(s-\theta),N]$ space for different values of the feedback strength η before and after the creation of this mode.

Figure 8(b) depicts the moment just before the creation of new ECM. In this case the phase space trajectory is mostly confined to the vicinity of MGM. The system visits the MGM many times before it is repelled across the unstable branch of the ellipse passing by the corresponding antimode. With increasing the feedback rate the period of RPP decreases. Just after the creation of a new pair of ECMs, in Fig. 8(c) we observe a dramatic change in the system trajectory around the ECMs. The system does not jump to the newly born MGM but most of the time it stays in the vicinity of the previous MGM. Then, surprisingly, from this mode the system follows the stable manifold of the new antimode. The system tries to hit this antimode making several loops close to it but before reaching it is repelled to the antimode of the previous MGM. As the feedback strength η increases, the system makes more and more turns around the new antimode and circles less and less frequently around the previous mode and the previous antimode; see Fig. 8(d). Finally, in Fig. 8(e) we come to the situation in which only one antimode is visited and the previous antimode does not play a role in the dynamics of RPP. Further increase of the feedback confines the trajectory closer and closer to the new MGM and increases the period of RPP. The stars in Figs. 8(b)–8(e) denote the moment in the phase trajectory for which the power drops to zero before slipping to one particulary chosen ECM — the MGM in Fig. 8(b). It takes for the system approximately the same time to travel from the maximum of the first peak in RPP to the moment indicated by stars for all cases from Fig. 8. Therefore, the change of the period of RPP is associated with the remaining part of the phase trajectory during one RPP and particularly with the complexity of the dynamics around the MGM and the nearby antimodes.

This behavior, in which the period of RPP exhibits a parabolic dependency on the feedback rate each time a new pair of ECMs is created, is not observed for larger values of the delay θ. As shown in Fig. 7(b), for $\theta=70$ T_{RPP} increases continuously when increasing the feedback rate η. This indicates that the period of RPP is sensitive to the delay or, in another words, the phase space configuration strongly modifies the dynamics of RPP in particular when there are only a few ECMs present in the system.

Since the structure of the external cavity plays a key role in the RPP dynamics we continue our investigations by checking the dependence of the period T_{RPP} of the envelope of RPP on the external cavity length. In Fig. 9 we plot $T_{\mathrm{RPP1}}(\theta)$ for different values of the current, namely $J=0.8$, 1.115, and 1.8. We observe that the injection current has much stronger impact on the period of RPP than the delay,

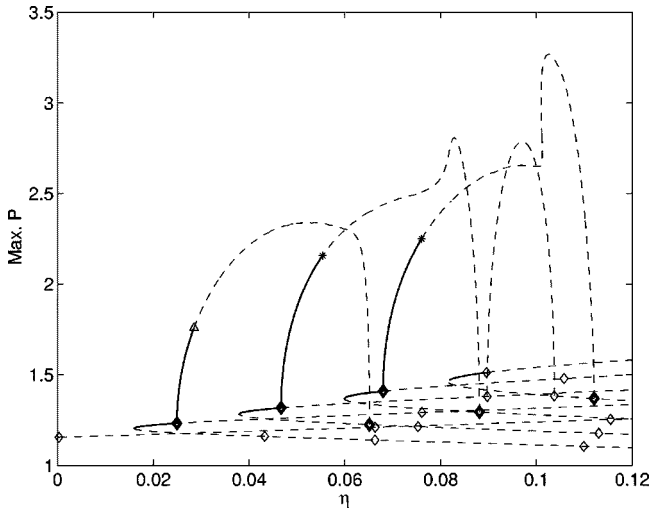

FIG. 10. Stability of ECMs and branches of time-periodic solutions in the route to RPP dynamics. Stable (unstable) branches of steady and time-periodic solutions are indicated in solid (dashed) lines. Diamonds indicate Hopf bifurcations, triangles are used for period doubling bifurcation and torus bifurcations are indicated by stars. The parameters are $J=1.155$, $\theta=70$, $\alpha=4$, and $\omega\theta=-\arctan\alpha$.

i.e., period changes in much broader range when changing the injection current. At large injection currents the RPP period is significantly smaller than the one at small currents. Moreover, we see that for each value of the injection current the dependency of T_{RPP1} on the delay time θ possesses a characteristic minimum. With increasing the current this minimum moves towards lower values of the delay. Interestingly, for each injection current the minimum of the RPP period occurs for the delays close to half of the RO period. Similarly to Fig. 7 the RPP period changes continuously for large delays whereas it is periodically interrupted for small delays in the vicinity of the creation of new ECMs, as visualized by the vertical lines. For larger θ new ECMs do not influence the dynamics of the RPP.

IV. BIFURCATION SIGNATURE OF RPP

We continue our numerical investigations of the LK equations by a systematic study of the global picture of bifurcations underlying the route to RPP dynamics. For that purpose we have used the continuation package DDE-BIFTOOL for delay-differential equations [32]. It allows to compute the stable and unstable branches of steady and time-periodic solutions. As already pointed out in recent works [20–24,26,33], the unstable branches of time-periodic solutions play an important role in our understanding of the global picture of bifurcations of the laser dynamics.

The bifurcation diagram obtained with this continuation method is plotted in Fig. 10. Only the first branches of steady states are shown. They appear in pairs as we increase the feedback rate η. Stable (unstable) parts of the branches are shown in solid (dashed) lines. The ECMs exhibit supercritical Hopf bifurcations. From these supercritical Hopf bifurcations emerge branches of time-periodic solutions. These branches of time-periodic solutions destabilize with a secondary bifurcation that can be either a period doubling bifurcation (as it is the case for the first plotted branch of time-periodic solution) or a torus bifurcation (as it is the case for the two other branches of time-periodic solutions plotted in Fig. 10). The unstable parts of the branches of time-periodic solutions always connect to a subcritical Hopf bifurcation located on the antimode branch of the next ECM. We say that the modes connect to the antimodes by forming Hopf bifurcation bridges. The two Hopf bifurcations which form each bridge are shown in bold. These bridges between ECMs through time-periodic solutions are very similar to those reported in Refs. [20–22,24,33]. However, interestingly, these branches of time-periodic solutions initiate a turning point and exhibit a more complex shape as we increase the feedback rate η. The first bridge between ECMs shown in Fig. 10 indeed exhibits a shape very different from that of the other, subsequent bridges. Moreover, the third plotted bridge between ECMs still connects a mode to an antimode but, in contrast to the two first bridges, it does not connect to the first Hopf bifurcation appearing on the antimode branch of the next ECM as η increases. Instead, it connects to the second Hopf bifurcation point on the antimode branch of the next ECM. As shown in Fig. 10, an unstable bridge of time-periodic solutions connects the first Hopf bifurcation on the antimode branch to another "unstable Hopf" bifurcation [21] located on the mode branch of a previous ECM solution. In the conventional bridge between a mode and an antimode [33] this first Hopf on the antimode branch would connect to a stable Hopf bifurcation on a mode branch, as shown in the two first bridges in Fig. 10. We therefore notice the appearance of a bifurcation bridge of a different topology as we increase the feedback rate η which coincides with the appearance of RPP dynamics.

The consequences of the topological change in the bifurcation diagram are shown in Fig. 11, which plots the bifurcation diagram of the laser intensity P for the same parameters than in Fig. 10 but obtained from a direct numerical integration of the LK equations. Indeed the complex dynamics emerging from the secondary bifurcations on the branches of time-periodic solutions cannot be followed with the continuation package DDE-BIFTOOL. As η increases from zero, the first ECM destabilizes with a Hopf bifurcation (symbol $\diamondsuit$). From this Hopf bifurcation emerges a branch of a time-periodic solution which destabilizes for larger values of η to period doubling and possibly chaotic oscillations. This first branch of time-periodic solutions for small values of η was not plotted in Fig. 10 and does not play a role in the emergence of RPP dynamics. If we further increase η, new ECMs are created and the laser exhibits a cascade of Hopf bifurcations from which emerge the branches of time-periodic solutions that we have plotted in Fig. 10 and that were identified as Hopf bifurcation bridges between a mode and the antimode of a next ECM solution. The bifurcation diagram of Fig. 11 shows that, in agreement with the stability analysis of the time-periodic solutions in Fig. 10, the three first bridges between ECMs exhibit either a period doubling bifurcation (the case of the first bridge) or a torus bifurcation (the case of the two next bridges) to a more complicated and irregular time dependency of the laser intensity. However the

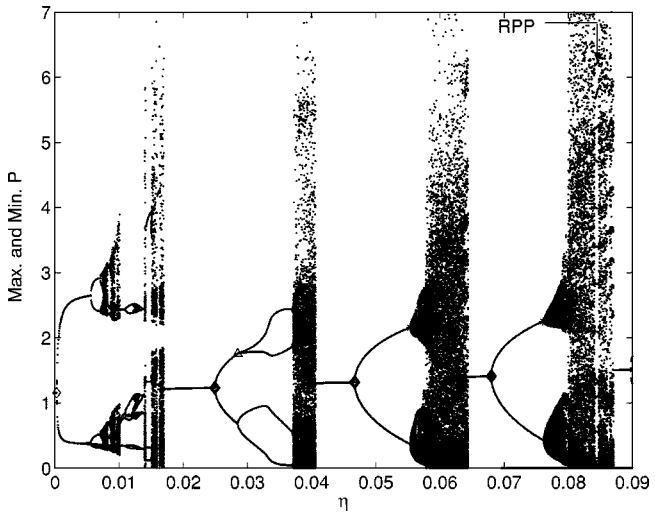

FIG. 11. Bifurcation diagram of P in the route to RPP dynamics, for the same parameters than in Fig. 10. This figure complements Fig. 10 in that it shows the complex dynamics that emerge after the time-periodic solutions have bifurcated. A window of RPP dynamics is shown with the arrow.

third bridge is very different in that we find a window of RPP dynamics in between two more irregular or chaotic intensity dynamics. This small region of RPP dynamics is indicated by the arrow in Fig. 11. The emergence of RPP occurs for values of η that correspond to a topological change in the bifurcation diagram.

The comparison between Fig. 10 and Fig. 11 therefore suggests that one of the bifurcation signature of RPP appears to be a Hopf bifurcation bridge between a mode and an antimode but in which the bridge connects to the second unstable Hopf bifurcation that appears on the antimode branch of the next ECM, in contrast to the previously reported types of mode-antimode bridges [20–24,33]. We have checked that this bifurcation signature of the RPP dynamics is present for several other sets of laser parameters.

V. CONCLUSIONS

We have studied the influence of delayed optical feedback from a short external cavity on the emission dynamics of semiconductor lasers using the Lang and Kobayashi rate equation model. We have presented the bifurcation scenario leading to RPP and we have given examples of bistability between RPP and time-periodic or steady state solutions. We have identified regions in feedback parameters space for which RPP occurs. We showed that by increasing the delay time the windows of RPP broaden, merge and finally shrink when the EC round-trip time approaches the RO period. Interestingly, the largest region of RPP occurs for delays around half of the RO period of the solitary laser. We also analyzed in detail the dependency of the period of the envelope of the pulse packages on the laser and feedback parameters. We found that the period of RPP exhibits a minimum for a delay time close to half of the RO period. The period of RPP increases in function of the feedback rate but for smaller delays the RPP period exhibits oscillations which we identify as being due to the destabilization of the RPP in the vicinity of newly born external cavity modes. Finally, we used recent continuation techniques for delay-differential equations to identify one of the bifurcation signature of RPP: the occurrence of RPP is accompanied by a dramatic change in the topology of the bifurcation diagram resulting in the creation of a new type of Hopf bifurcation bridge between a stable ECM and an unstable saddle-type ECM.

ACKNOWLEDGMENTS

The authors acknowledge the support of the FNRS (Belgium), the IAP Program of the Belgian government, as well as FWO-Flanders, GOA, OZR of the VUB, the EU project SLAM, and COST Action 288 “Nanoscale and ultrafast photonics”.

[1] R. F. Broom, E. Mohn, C. Rish, and R. Salathé, IEEE J. Quantum Electron. **QE-6**, 328 (1970).
[2] C. Masoller and N. B. Abraham, Phys. Rev. A **57**, 1313 (1998).
[3] J. Mørk and B. Tromborg, IEEE Photonics Technol. Lett. **2**, 21 (1990).
[4] K. Petermann, IEEE J. Sel. Top. Quantum Electron. **1**, 480 (1995).
[5] T. L. Paoli and J. E. Ripper, IEEE J. Quantum Electron. **QE-6**, 335 (1970).
[6] G. P. Agraval, IEEE J. Quantum Electron. **20**, 468 (1984).
[7] I. Fischer, Y. Liu, and P. Davis, Phys. Rev. A **62**, 011801 (2000).
[8] P. Ruprecht and J. Brandenberger, Opt. Commun. **93**, 82 (1992).
[9] K. Koltyś, A. Tabaka, V. Gómez, H. Thienpont, and K. Panajotov, Proceedings of IEEE/LEOS, Benelux Chapter, 2003, pp. 109–112, available at http://leosbenelux.org/symp03/s03p109.pdf
[10] R. Lang and K. Kobayashi, IEEE J. Quantum Electron. **16**, 347 (1980).
[11] P. M. Alsing, V. Kovanis, A. Gavrielides, and T. Erneux, Phys. Rev. A **53**, 4429 (1996).
[12] C. H. Henry and R. F. Kazarinov, IEEE J. Quantum Electron. **QE-22**, 294 (1986).
[13] R. W. Tkach and A. R Chraplyvy, J. Lightwave Technol. **LT-4** 1655 (1986).
[14] A. Tager and B. Elenkrig, IEEE J. Quantum Electron. **29**, 2886 (1994).
[15] T. Heil, I. Fischer, W. Elsäßer, and A. Gavrielides, Phys. Rev. Lett. **87**, 243901 (2001).
[16] C. Risch, C. Voumard, F. K. Reinhart, and R. Salathé, IEEE J. Quantum Electron. **QE-22**, 294 (1986).
[17] C. Risch and C. Voumard, J. Appl. Phys. **48**, 2083 (1977).

[18] D. Lenstra, B. Verbeek, and A. den Boef, IEEE J. Quantum Electron. **21**, 674 (1985).
[19] A. Tager and K. Petermann, IEEE J. Quantum Electron. **30**, 1553 (1994).
[20] M. Sciamanna, F. Rogister, O. Deparis, P. Mégret, M. Blondel, and T. Erneux, Opt. Lett. **27**, 261 (2002).
[21] M. Sciamanna, T. Erneux, F. Rogister, O. Deparis, P. Mégret, and M. Blondel, Phys. Rev. A **65**, 041801(R) (2002).
[22] T. Erneux, A. Gavrielides, and M. Sciamanna, Phys. Rev. A **66**, 033809 (2002).
[23] M. Sciamanna, T. Erneux, A. Gavrielides, V. Kovanis, P. Mégret, and M. Blondel, in *Physics and Simulation of Optoelectronic Devices XI*, edited by M. Osinski, H. Amano, and P. Blood [Proc. SPIE **4986**, 469 (2003)].
[24] M. Sciamanna, Ph.D thesis, Faculty Polytechnique de Mons, Belgium, 2004.
[25] Y. Ikuma and J. Ohtsubo, IEEE J. Quantum Electron. **34**, 1240 (1998).
[26] T. Heil, I. Fischer, W. Elsäßer, B. Krauskopf, K. Green, and A. Gavrielides, Phys. Rev. E **67**, 066214 (2003).
[27] T. Sano, Phys. Rev. A **50**, 2719 (1994).
[28] C. Grebogi, E. Ott, and J. A. Yorke, Phys. Rev. Lett. **48**, 1507 (1982).
[29] A. Tabaka, M. Sciamanna, I. Veretennicoff, and K. Panajotov, in *Proceedings of SPIE Photonics Europe, Semiconductor Lasers and Laser Dynamics*, edited by D. Lenstra, G. Morthier, T. Erneux, and M. Pessa [Proc. SPIE **5452**, 93 (2004)].
[30] M. Fujiwara, K. Kubota, and R. Lang, Appl. Phys. Lett. **38**, 217 (1981).
[31] R. J. Jones, P. Spencer, J. Lawrence, and D. Kane, IEE Proc.: Optoelectron. **148**, 7 (2001).
[32] K. Engelborghs, T. Luzyanina, and D. Roose, tW-330, URL http://www.cs-kuleuven.ac.be/koen/delay/ddebiftool.shtm1 (2000).
[33] D. Pieroux, T. Erneux, B. Haegeman, K. Engelborghs, and D. Roose, Phys. Rev. Lett. **87**, 193901 (2001).